6th Internatinal Workshop on Atmospheric Science from Space using Fourier Transform Spectrometry (ASSFTS)

San Juan Institute
San Juan Capistrano
California, USA

October 3, 4 and 5 1995

SUMMARY

Infrared Atmospheric Sounding Interferometer (IASI) performance evaluation

F. Hénault, D. Miras, D. Scheidel, and F. Boubault

AEROSPATIALE CANNES, 100, Boulevard du Midi, BP 99
06322 CANNES LA BOCCA, FRANCE

ABSTRACT

The IASI instrument (Infrared Atmospheric Sounding Interferometer) is a Fourier-transform interferometer which will be launched on the European METOP meteorological platform, in order to provide spectrums of the Earth's atmosphere seen from space. The data acquired by the instrument will be ground-processed in order to derive accurate measurements of the temperature, humidity, and composition of the atmosphere. The French National Agency (CNES) is directing the development phase of the IASI instrument. Studies of its performances were undertaken with AEROSPATIALE as subcontractor since 1994.

The purpose of the communication is to expose the main principles on which the IASI instrument performances have been evaluated during the two previous years. Instrument requirements are set upon different types of performance (geometrical, spectral, radiometric noise, and radiometric calibration), which dictated the development of evoluted simulation tools. This involves the modelisation of several characteristic functions (interferometer transmission and contrast, self-apodization) that may affect different performances at the same time.

The field of view of the instrument and the contrast of the interferometer are evaluated by means of ray-tracing programs. These functions are used as inputs for the spectral model.

The spectral model requires the evaluation of the complex self-apodization function, and takes into account various families of errors such as instrument field of view decentring, lateral shifts of the interferometer cornercubes, sampling jitter, influence of the reference laser... Spectral performance may also be affected by the on-board processing algorithms.

Radiometric performance consists in radiometric noise and accuracies of the brightness measurements performed by the instrument (absolute, relative, and repeatabilities). The latter require a complex calibration processing. They again involve the contrast function and sampling jitter. The influences of the electronic acquisition chain, the scanning mirror reflectivity, the characteristics of the on-board calibration blackbody, and the instrument self-emission are also taken into account.

Each different type of instrument requirements is illustrated by some numerical results or performance budgets derived from the present design of the IASI instrument.

1. INTRODUCTION

The IASI instrument (Infrared Atmospheric Sounding Interferometer) is a Fourier-transform spectrometer (FTS) which will be launched on the european METOP meteorological platform, in order to provide spectrums of the Earth's atmosphere observed from space. The data acquired by the instrument will be ground-processed in order to derive accurate measurements of the temperature, humidity, and composition of the atmosphere. The French National Agency (CNES) is directing the development phase of the IASI instrument. The evaluation of the instrument performance with respect to its specification was undertaken with AEROSPATIALE as subcontractor two years ago. The purpose of the communication is to present the main results of these studies.

After a quick glance at the instrument requirements, the baselines for the developments of the different performance evaluation models are exposed. They evidence the influence of the interferogram contrast function and the self-apodization function on both spectral and radiometric performances. Evaluating these two characteristic functions requires that an interface with a geometrical ray-tracing model is implemented, in order to provide some necessary inputs such as instrument actual field of view (FOV) and interferometer wavefront errors.

Once the instrument FOV and contrast function are known, the spectral and radiometric performances are evaluated independently, from analytical expressions which do not involve the use of heavy mathematical models. The evaluation methods of the different instrument performances are summarised in the last paragraphs, and some preliminary conclusions are then drawn.

2. THE IASI INSTRUMENT AND ITS PERFORMANCE MODELS

The IASI instrument and its specifications, as well as its various subsystems, were presented during the 5th International Workshop on ASSFTS [RD1]. The purpose of this paragraph is to sum up the main performance requirements of the instrument, and the basic principles on which its performance models will be built.

2.1 REQUIREMENTS

2.1.1 Geometrical performance

The theoretical IASI field of view is constituted of four circular pixels, which centres are located at ± 10.815 mrad from the nominal optical axis, and diameters are equal to 14.35 mrad. They may also be considered as the Instrument Point Spread Functions (IPSF) including the size of the detectors.

The IPSF must be characterised (by means of tests) up to field angles such that 99 % of the total incident energy effectively reach the detectors. The diffused energy between neighbouring pixels (pixel crosstalk), as well as IPSF spectral uniformity between the three spectral bands of the instrument, are subject to specifications that are summarised in the table below.

Spectral Band	**B1**		**B2**		**B3**		**Unit**
Wavenumbers	650	1000	1250	1650	2150	2450	cm^{-1}
Pixel crosstalk	0.5	0.5	0.75	0.75	1	1	%
Spectral uniformity	0.4	0.4	0.4	0.4	0.4	0.4	%

2.1.2 Spectral performance

The spectral performance requirements are all applicable to the so-called Instrument Spectral Response Function (ISRF), which is the spectral radiance distribution measured by the instrument observing an ideal monochromatic light source of wavenumber σ. The ISRF must be characterised within a spectral channel of $[\sigma - 16\ cm^{-1}, \sigma + 16\ cm^{-1}]$. Perturbations of the ISRF outside the channel are considered as parasitic contributions of higher frequency.

Spectral requirements inside the channels apply to the spectral resolution, the spectral calibration, and the ISRF shape deformation, that is estimated by means of a shape index. These notions are illustrated in the figure 1.

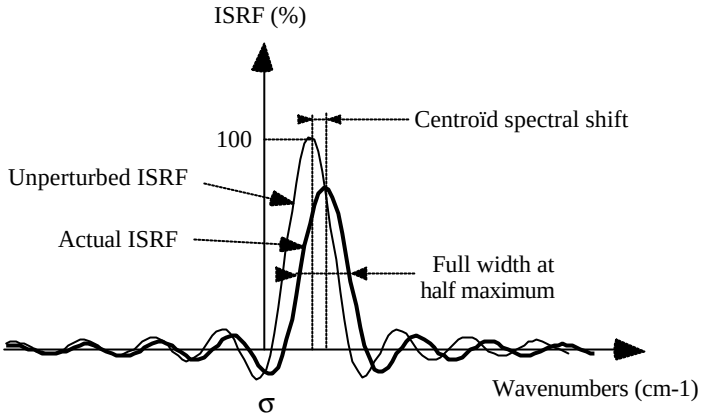

Figure 1 : The ISRF function and its main requirements

The spectral resolution is the full width at half maximum (FWHM) of the Spectral Response Function. The spectral calibration is the spectral shift of the ISRF centre, when the instrument is affected by short-term perturbations, with respect to the last reference ISRF curve (the instrument is periodically calibrated in-flight). Finally, the shape index is a number proportional to the deformation of the curve (both centroïds being merged).

The out-of-channel parasitic contributions mainly affect the radiometric performance, but can only be evaluated through spectral measurements. They may have a random or periodic origin, and are therefore subjected to different requirements.

The main spectral requirements of the instrument are summarised in the table below.

Spectral Band	**B1**		**B2**		**B3**		**Unit**
Wavenumbers	650	1000	1250	1650	2150	2450	cm^{-1}
Spectral resolution	0.35	0.35	0.45	0.45	0.55	0.55	cm^{-1}
Spectral calibration	$0.65\ 10^{-3}$	$1.\ 10^{-3}$	$1.25\ 10^{-3}$	$1.65\ 10^{-3}$	$2.15\ 10^{-3}$	$2.45\ 10^{-3}$	cm^{-1}
Shape index	1	1	2	2	3	3	%
Random perturbations	1	1	1	1	1	1	%

2.1.3 Radiometric noise performance

The radiometric noise is specified in terms of Noise Equivalent Temperature difference (NEdT), at a blackbody temperature of 280 K. For different scene temperatures, the specification corresponds to the same Noise Equivalent Brightness difference (NEdL). It includes all the noise sources originating from both the electronic or the optics, that could be measured on-ground if the IASI instrument was observing a spatially-uniform blackbody. The required values are given in the table below, however it must be noticed that the specification can be relaxed at the upper end of each spectral band.

Spectral Band	**B1**		**B2**		**B3**		**Unit**
Wavenumbers	650	1000	1250	1650	2150	2450	cm^{-1}
Radiometric noise	0.25	0.25	0.25	0.25	0.4	0.4	K

2.1.4 Radiometric calibration performance

The radiometric calibration specification is divided into three parts:

1) The absolute accuracy denotes the difference between any equivalent temperature estimate measured at any time during the instrument's lifetime and the actual equivalent temperature of the observed scene. It must be lower than 0.5 K.

2) The repeatabilities denote the difference between two temperatures estimates measured off an unchanged scene at different times scales :

- Instantaneous repeatability corresponding to a few acquisition cycles (duration of one cycle is 8 seconds).
- Orbital repeatability corresponding to the duration of one orbit (around 110 minutes).
- Ageing repeatability corresponding to the whole life of the instrument.

The repeatabilities performance must be better than 0.15 K.

3) The relative accuracies which also are composed of three subrequirements :

- Scan mirror relative accuracy is the difference between equivalent temperatures of the scene observed under different mirror angles.
- Interpixels relative accuracy is the difference between temperatures measured by the four pixels.
- Interbands relative accuracy is the difference between temperatures measured within the three spectral bands.

The relative accuracies performance must be better than 0.1 K.

2.2 PERFORMANCE MODELS

The basic principles of the IASI instrument are detailed in [RD2]. It is a Fourier transform interferometer which presents the spectral information in the form of an interferogram recorded while varying the Optical Path Difference (OPD) between the arms of a Michelson interferometer equipped with cornercubes. The optical layout of the instrument is illustrated on the figure 2. The interferogram is formed on a detector which is imaged with the cornercubes and the entrance pupil of the instrument (located on the Scan mirror) through intermediate optics. The dimension of the pupil is defined by an internal aperture stop. The rays coming from the Earth are focused at the interferometer focal plane, where a field stop limits the instrumental FOV, and then are spread over all the detector surface. Therefore the interferogram can be considered as the sum of all the interfering rays coming from both arms of the interferometer, and then passing through the whole field and aperture stops areas.

Let us consider a monochromatic beam arriving on the interferometer at the wavenumber σ, and let ξ be the OPD resulting from the mechanical displacement of the moving cornercube along the optical axis of the interferometer. The resulting intensity $I(\xi)$ of the interferogram recorded on the detector then has the most general form :

$$I(\xi)=T(\sigma)\left\{1+\mathrm{Real}\left[\mathbf{C}(\sigma)\mathbf{V}_{\sigma}(\xi)e^{2i\pi\sigma\xi}\right]\right\} \qquad (2.1)$$

where $T(\sigma)$ is the transmission of the optics (including the interferometer), $\mathbf{C}(\sigma)$ is the depth of modulation (contrast) of the interferogram, and $\mathbf{V}_{\sigma}(\xi)$ is the self-apodization function of the instrument (the bold characters denote complex functions, and Real[ ] the extraction of their real part). The Spectral Response Function (ISRF) of the instrument at the wavenumber σ' is obtained through the Fourier transform of the $\mathbf{V}_{\sigma}(\xi)$ function :

$$\mathbf{SRF}_{\sigma'}(\sigma)=\mathrm{Real}\left\{FT\left[\mathbf{V}_{\sigma'}(\xi)\right](\sigma)\right\} \qquad (2.2)$$

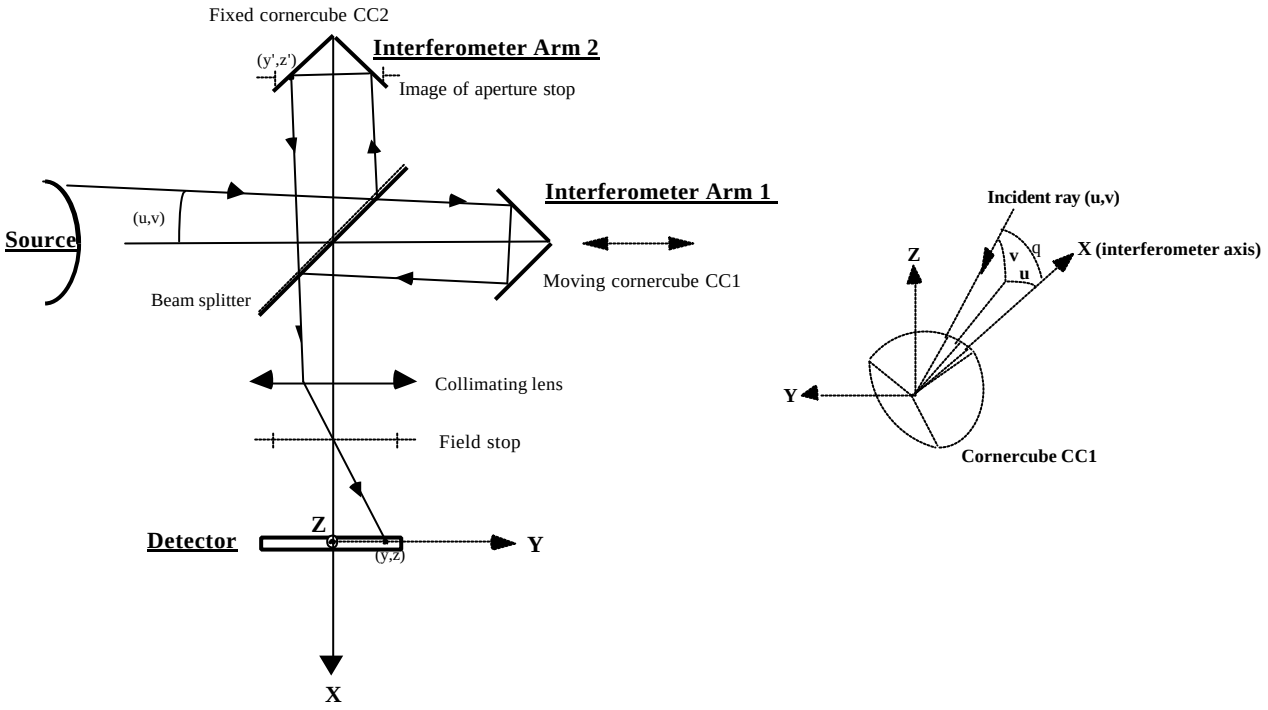

Figure 2 : Interfering rays and field angles in the IASI interferometer

The basic assumption is to state that the interferogram contrast function does not vary noticeably over the whole instrument FOV, which allows to separate the contrast from the self-apodization function, and thus the radiometric performance from the spectral performance. Therefore the model is principally built around both the contrast and instrument self-apodization functions. The links with the spectral and radiometric performance budgets and their requirements, as well as other existing models (mainly the geometrical model) are shown in the figure 3.

At a first glance, the architecture of the performance simulator may seem rather complicated, so a few essential points are now highlighted.

1) A classical ray-tracing geometrical model of the instrument is firstly implemented. One of its main outputs are the maps of transmittances of the instrument for different angles of the incident beam, thus defining the actual FOV (or IPSF) of the interferometer, which is a basic input for the evaluation of the self-apodization function and the whole spectral performance. The IPSF requirements obviously are verified at this moment. The geometrical model also provides the WFEs reflected along the two arms of the interferometer, from which the contrast function $\mathbf{C}(\sigma)$ can be computed either using intermediate WFE files, either directly. At this stage, only a ray-tracing program has the ability to include the various error sources which may contribute to the degradation of the IPSF (defocus, vignetting...) or the contrast function (beamsplitter and cornercubes defects) taking into account the actual optical lay-out of the instrument.

2) Once the IPSF maps are available, the self-apodization function is computed. This calculation includes the evaluation of the OPD, and consists in a numerical integration over the pixel FOVs. No ray-tracing is involved within this operation. Fourier-transforming of the self-apodization function finally leads to the Instrument Spectral Response Function, and thus to all the diagnostics values (spectral calibration, shape index...) characterising the spectral performance.

3) Meanwhile the contrast function $\mathbf{C}(\sigma)$ is directly entered within the radiometric noise model, as well as the instrument spectral responsivity and the optics transmission (the latter may also be evaluated using the geometrical model libraries).

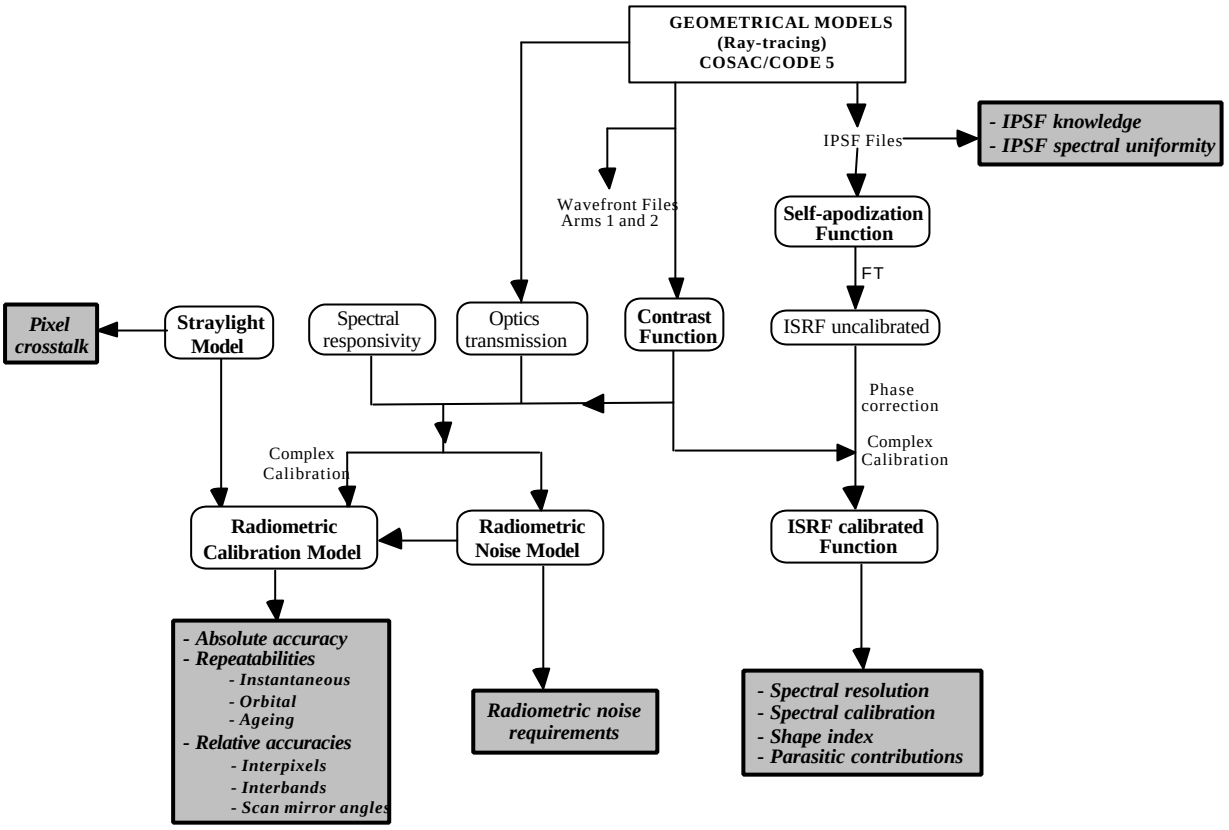

Figure 3 : Links between spectral, geometrical, and radiometric models. Instrument specifications are indicated within the grey boxes

4) The radiometric noise itself is a direct input of the radiometric calibration model, as the noise affecting the reference measurements (cold and hot blackbodies) induces calibration uncertainties. At the same time, drifts or bias errors of the spectral responsivity, the optics transmission, or the contrast function also contribute to the degradation of the radiometric calibration performance. Finally the instrument straylight studies will provide additional errors terms to be included within the radiometric budget.

It must be noticed that this approach differs noticeably from the global ray-tracing calculations that are sometimes employed in order to evaluate the performances of a FTS. It presents the advantage of being less heavy, and therefore it does not require excessive computing times. The association of a ray-tracing software with several numerical simulations and performance budgets allows to enter the actual optical configuration of the instrument including a wide range of error sources. The calculation of the contrast function takes a few minutes, and an ISRF is obtained in a few seconds only. This high reduction of the needed computing times is due to the basic assumption described hereabove. Its validity may be assessed by comparison with the results of a heavier mathematical models, such as that developed by the CNES [RD1].

The next paragraphs will now provide some details about the main instrument performance models.

3. THE INSTRUMENT GEOMETRICAL MODEL

Up to now, two geometrical models were used in order to perform the IASI ray-tracing calculations. The first is the well-known CODE 5 program, while the second, named COSAC, was specially developed for the IASI instrument, and required the introduction of non-sequential ray-tracing in order to model the reflections inside the cornercubes. The numerical results provided by both software are saved in the CODE 5 standard INT files, thus making easy to use indifferently the two programs in order to compare their results.

Evaluation of the contrast function

The modulus of the contrast function **C**(σ) varies between 0 and 1, depending upon transmittance and image quality of the interferometer, and most likely on polarisation. The basic relationship used for the evaluation of the contrast function includes the WFEs originating from both arms of the interferometer. Due to the presence of the cornercubes, which will divide the surface of the pupil into 6 different subpupils areas, it is not possible to derive simple analytical expressions of these wavefront errors, and therefore a ray-tracing evaluation is required. Thus it becomes possible to introduce various types of defects on the cornercubes and the beamsplitter plates : tilts or parallelism defects, spherical, cylindrical or higher-order deformations, cornercubes position and orientation errors, thickness difference between separator and compensator plates of the beamsplitter... The first results provided by the contrast function simulator tend to confirm the assumptions on which the whole performance model is based. In particular, it has been noticed that the contrast do not depend on the axial position of the moving cornercube, and that its variations with respect to the cornercube lateral shifts are negligible. However, the main hypothesis was to state that the contrast does not depend significantly on the angles of the incident beam, thus separating the contrast function from the self-apodization function. This assumption was verified by computing the contrast function for six different directions within the IASI field of view. The first direction is fictive and corresponds to the instrument FOV centre. The second point is the centre of one IASI pixel, and the four other directions are located at the pixel edges.

The complex contrast function was evaluated while introducing an angular defect of 0.01 mrad on one reflecting face of the cornercube. A 3D view of the resulting WFE is shown in the figure 4. The numerical results are presented in the figure 5. It can be seen that the dependence of the contrast function with respect to the field angles subtended by the IASI pixel does not exceed 0.01 for typical contrast values of 0.9. Therefore the independence assumption is considered as valid.

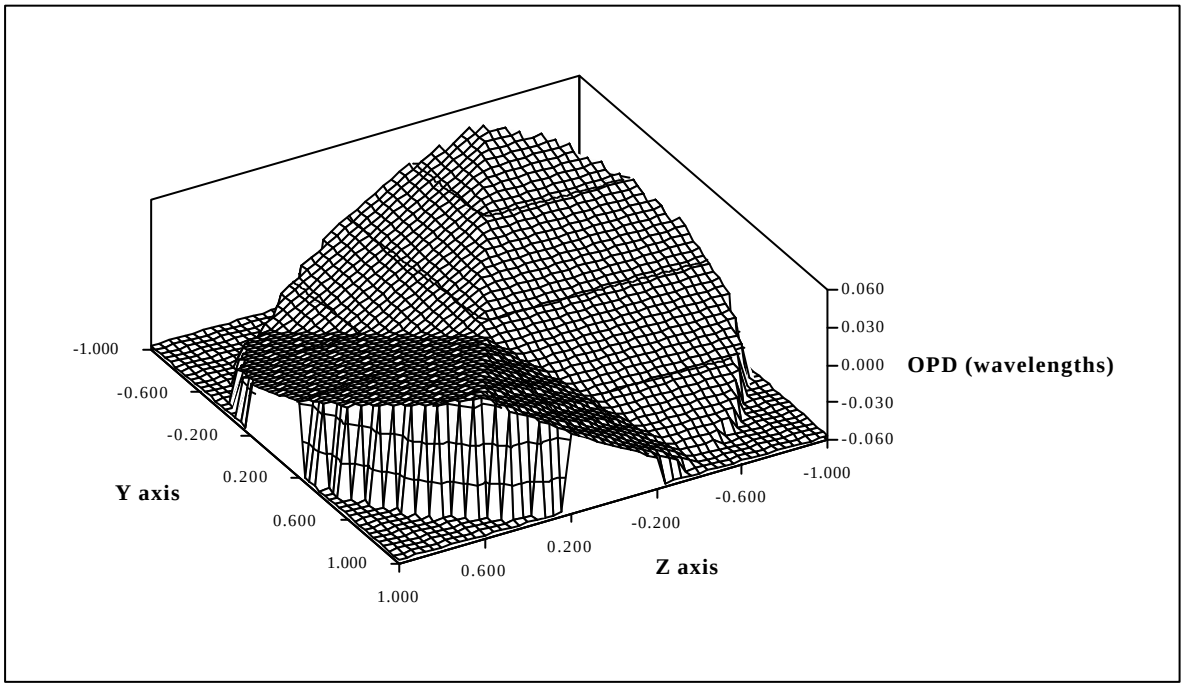

Figure 4 : Wavefront error resulting from a 0.01 mrad angular defect of the cornercube
(PTV = 0.113 λ, RMS = 0.023 λ, with λ = 8 μm)

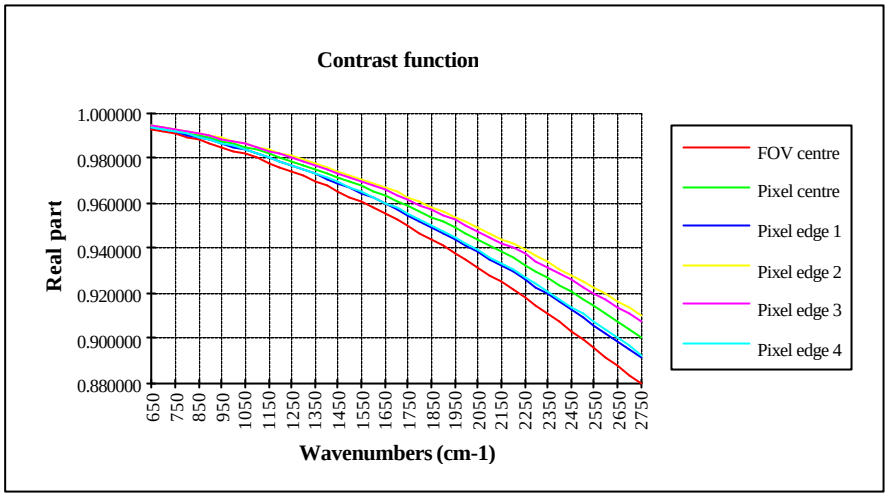

5.a)

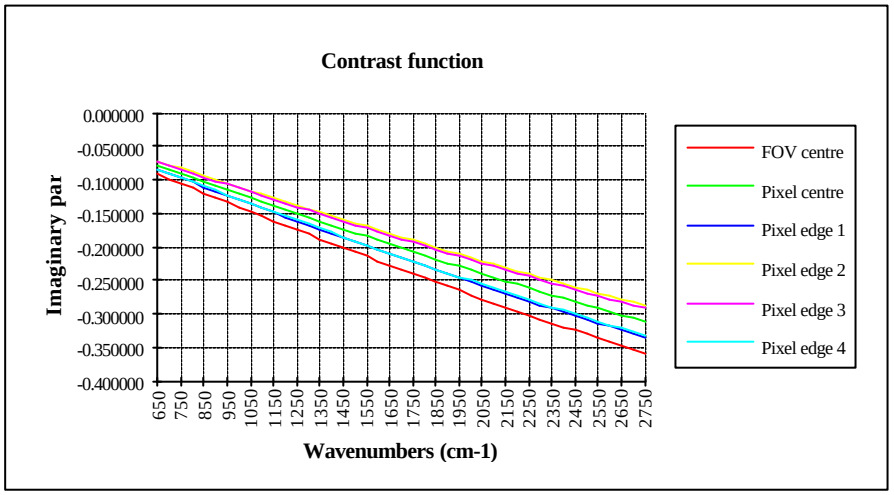

5.b)

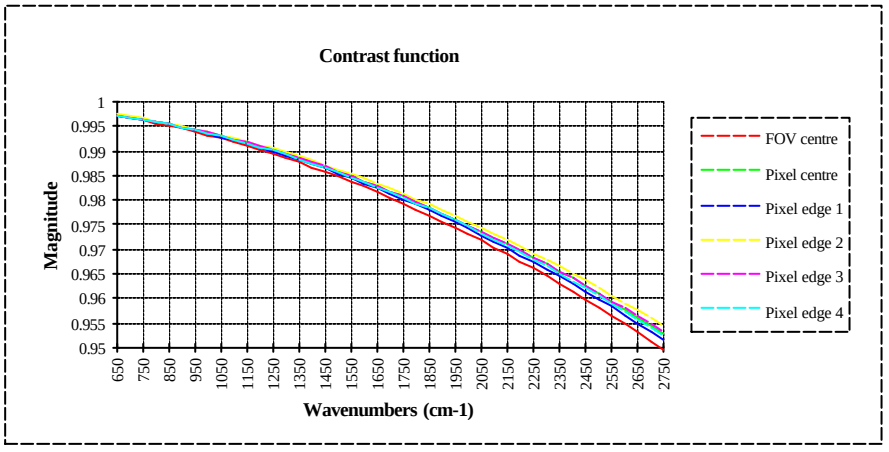

5.c)

Figure 5 : Interferogram contrast function obtained with a 0.01 mrad angular defect of the cornercube.
5.a) Real part; 5.b) Imaginary part; 5.c) Magnitude

4. THE SPECTRAL MODEL

4.1 PRINCIPLE

As already seen in relation (2.2), the Spectral Response Function of the instrument at the wavemumber σ is obtained by the direct Fourier Transform of the complex self-apodization function $\mathbf{V}_\sigma(\xi)$ of the interferogram. $\mathbf{V}_\sigma(\xi)$ depends on the axial position of the moving cornercube and is calculated without ray-tracing, using a summation over all the instrument FOV and an analytical development of the interferometer Optical Path Difference (OPD). The simulator takes into account three different families of instrumental defects, that are listed below. The effects of the on-board data processing algorithms (see figure 10) are also discussed there.

Field of view decentring effects

These angular shifts of the instrument FOV resulting from translations or rotations of some optical components inside the instrument (such as beamsplitter, mirrors located between the beamsplitter and the cold optics, or the cold optics subsystem itself) directly affect the spectral performance. They may be deduced either by first-order analysis, either using a ray-tracing computing code.

Cornercubes lateral shifts

The IASI instrument may present a type of misalignment known as the cornercube lateral shift defect, varying when the cornercube moves along the interferometer optical axis. Thus different types of lateral shift variations may be considered : constant, parabolic, periodic... It can be shown that the special case of linear variations (which corresponds to a tilt of the cornercube displacement with respect to the interferometer optical axis) strictly is equivalent to a field of view decentring. Obviously, cornercube lateral shifs may originate from the misalignments of some optical components such as the beamsplitter.

Sampling jitter

In the IASI interferometer, the axial distance of the moving cornercube is measured using the interference pattern of a very stable laser beam. Random or periodic errors in the interferometer scan speed and instability of the reference laser are referred to as “jitter”. Its study may be based upon theoretical works, but it can also directly be introduced within the ISRF numerical model using a simplified algorithm. Error terms related to the misalignments of the reference laser also are taken into account.

Phase correction

Most generally, the Fourier transforms of the interferograms recorded by a FTS are not true real functions, but also have an imaginary part. This may be due to a shift ξ_0 of the centerburst of the interferogram with respect to its first point, or to some typical instrumental errors. Then a phase-correction algorithm has to be used in order to recover most of the spectral information within the real part of the raw spectrum. Several methods of phase-correction have already been studied in the cases of large spectrums [RD3]. However in the case of the IASI SRF calculations, one may consider that the ISRFs do not need to be phase-corrected, because it is assumed that over such narrow spectral domains the phase simply acts as a constant multiplying factor.

Complex calibration

Although the complex calibration procedure is more related to the radiometric performance than to the spectral performance, it will be included within the ISRF simulations, because the IASI ISRFs measured during the instrument test sequence will actually be obtained once the complex calibration processing is completed. Therefore it is necessary to verify if the spectral performances are affected by this procedure. The principle of the radiometric complex calibration is explained in the paragraph 6. In the case of ISRF simulations however, it is not foreseen to introduce the beamsplitter parasitic spectrum, nor the drifts errors occurring during a typical calibration sequence. Thus the spectral radiance measured during the observation of the cold reference blackbody will be set to zero.

4.2 NUMERICAL RESULTS / COMPARISON WITH OTHER MODELS

The results of our ISRF simulator (numerical model) were compared with those obtained using the CNES mathematical model, which is based upon intensive ray-tracing [RD1]. The perturbations introduced within the IASI instrument are denoted using the acronyms listed in the next page.

Two critical performances (spectral calibration and shape index) were selected for the comparison. The results obtained using both numerical and mathematical models are presented in the figures 6 and 7. They show the evolution of the spectral performances at different wavenumbers by means of histograms. It can be seen that the numerical and mathematical models both lead to comparable results and tendancies, although their basic principles are much different. As the mathematical model should be considered as a reference, the validity of the numerical model described herein is then assessed.

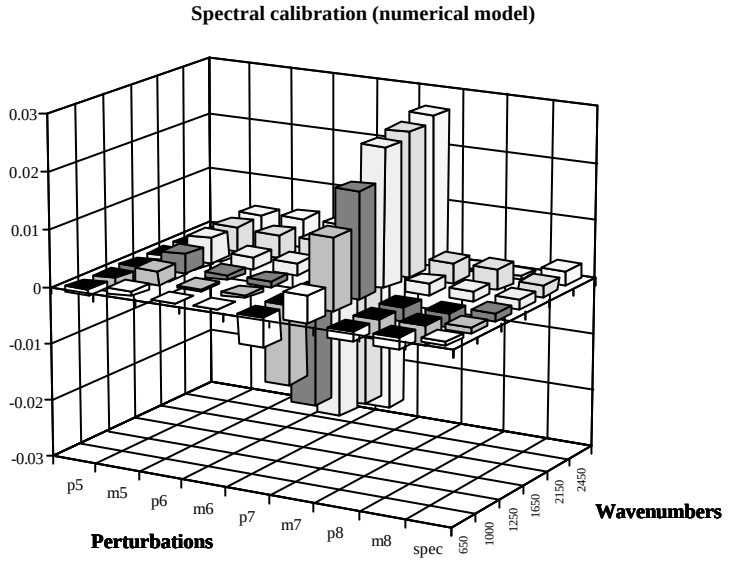

6.a)

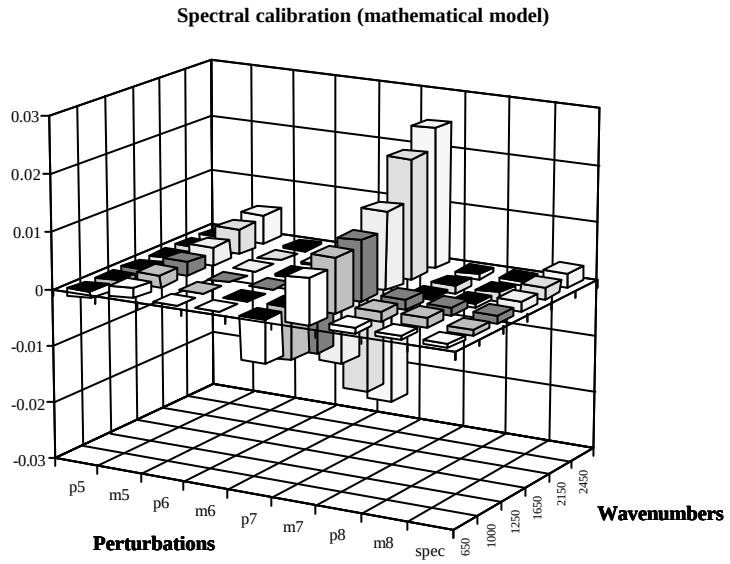

6.b)

Figure 6 : Spectral calibration performance evaluated using : 6.a) Numerical model ; 6.b) Mathematical model

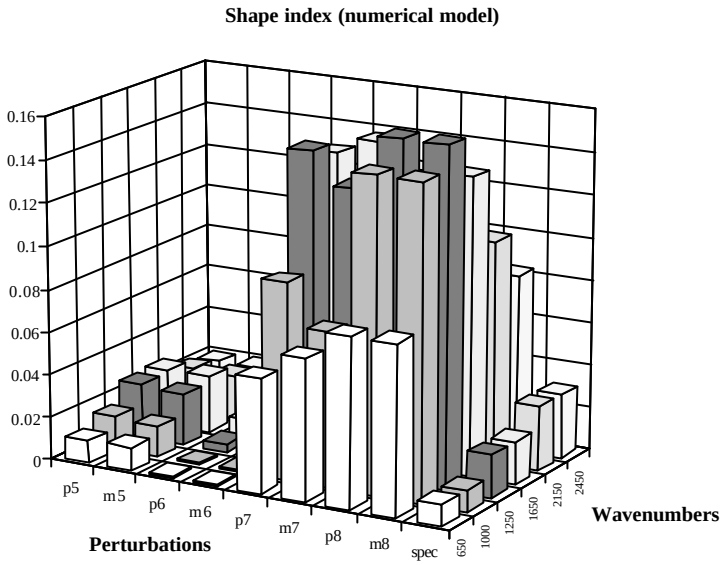

7.a)

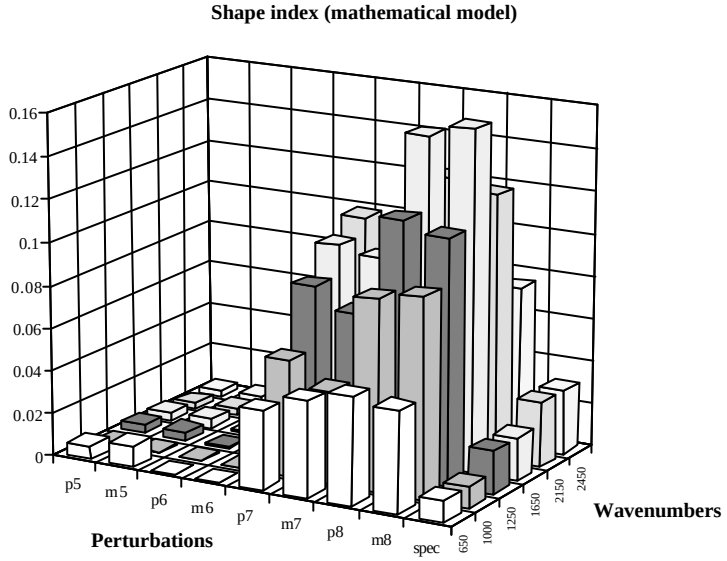

7.b)

Figure 7 : Shape index performance evaluated using : 7.a) Numerical model ; 7.b) Mathematical model

Acronyms	Perturbations
p5	Cold optics decentring of +100 µm along Z axis
m5	Cold optics decentring of -100 µm along Z axis
p6	Constant lateral shift of the moving cornercube of +10 µm along Z axis
m6	Constant lateral shift of the moving cornercube of -10 µm along Z axis
p7	Linear lateral shift of the moving cornercube of +10 µm along Z axis
m7	Linear lateral shift of the moving cornercube of -10 µm along Z axis
p8	Parabolic lateral shift of the moving cornercube of +25 µm along Z axis
m8	Parabolic lateral shift of the moving cornercube of -25 µm along Z axis
spec	Instrument specification as defined in § 2.1.2

5. THE RADIOMETRIC NOISE MODEL

5.1 PRINCIPLE

According to [RD3] the expression of the radiometric noise NEdL(σ) affecting the measurements performed by the IASI instrument is the following :

$$NEdL(\sigma) = \frac{NEP}{\sqrt{N\ \Delta\sigma}} \times \frac{\sqrt{2\, v_{CC}\ \sigma_{Max}}}{G\ T(\sigma) \left|\mathbf{R}(\sigma)\right| \left|\mathbf{C}(\sigma)\right|} \qquad (5.1)$$

where
- NEP : Noise Equivalent Power of the acquisition chain
- v_{CC} : Cornercube scan speed
- σ_{Max} : Maximal wavenumber in spectral band
- N : Number of samples within the IASI interferograms
- $\Delta\sigma$: Channels spectral width
- G : Geometrical étendue of the instrument
- $\mathbf{R}(\sigma)$: Complex spectral responsivity function of the instrument

Based upon the previous relationship, a detailed error budget of the radiometric noise was developed, taking into account actual subsystem designs. The optics transmission and the contrast function of the interferogram both affect noise performance since they reduce the spectral signal while not affecting the noise, thus some elements of specifications of the interferometer subsystem and the beamsplitter (image quality, transmission factors...) may directly be derived from the radiometric noise requirements. The radiometric noise is computed in five steps :

- Subsystems noise computing from specified parameters or first design results.
- Global NEP per band calculation.
- Total IASI input equivalent noise computing and NEP / NEdL / NEdT translation :

$$NEdT(\sigma) = \frac{NEdL(\sigma)}{\partial L_{BB} / \partial T \Big|_{T,\sigma}} \qquad (5.2)$$

- Instrument noise per spectral channel deduction.
- Processing noise addition.

5.2 CURRENT RESULTS

Instrument NEdT performance is presented in the figure 8 associated with the specified three bands limits. Noise figure is computed in the worst 280 K source temperature case.

Band B1 and B2 detectors are HgCdTe while band B3 are InSb type. B1 detectors are photoconductives producing in this way a considerable part of the noise budget due to the bias current shot noise. However for this band the final noise performance is within the IASI specification.

Even if the source radiance and the detectors responses are lower for band B2, the noise budget is better than for B1 because photovoltaic technology is used there. Without strong bias current, photovoltaic devices offer better performance than PC at these wavelengths. NEdT is degraded out of the IASI B2 specified NEdT segment, due to the rapid fall of detectors responsivity shape.

For B3, we note that the performance deteriorates above 2250 cm^{-1} due to the rapid fall in source radiance conjugated with a lower photovoltaic detector response. This figure is degraded by the high preamplifier gain associated with substantial parasitic detector capacitance.

The radiometric budget should not be considered as dramatic at the extreme end of each band since the digital processing has the ability to select the best SNR in such band overlay areas.

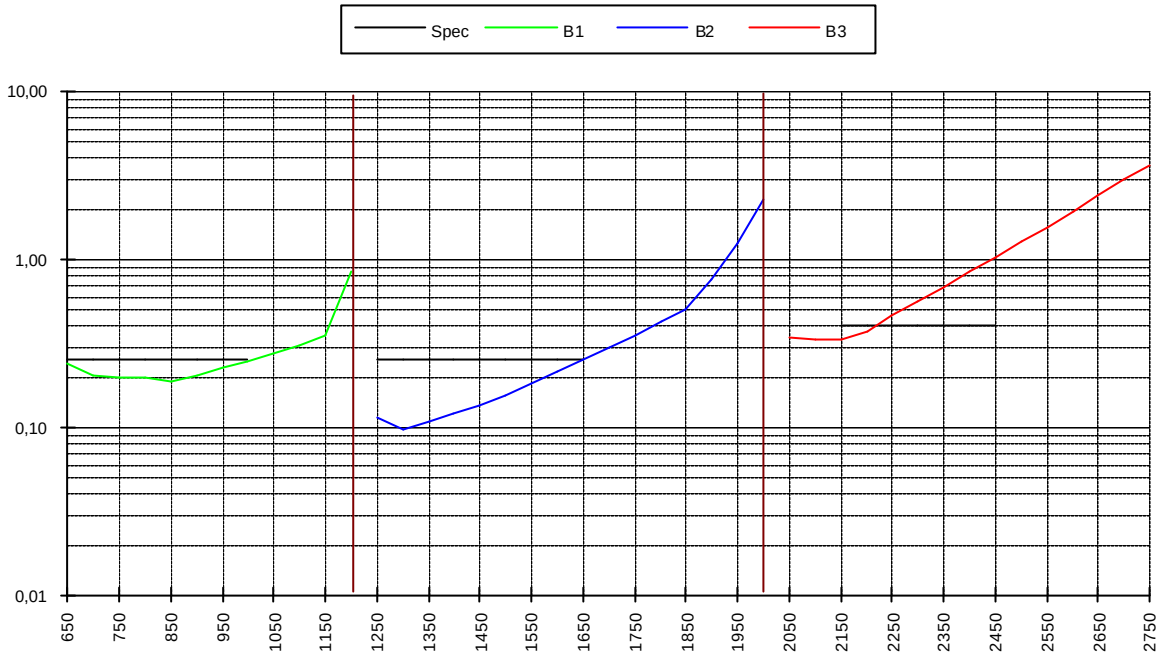

Figure 8 : Instrument radiometric noise performance

6. THE RADIOMETRIC CALIBRATION MODEL

6.1 PRINCIPLE

Once an interferogram is acquired, it will be submitted to a sophisticated data processing (the main part of which is performed on-board) in order to retrieve the raw complex spectrums $\mathbf{S}(\sigma)$ in a first time, and then the real calibrated spectral radiances $L(\sigma)$. This is the purpose of the radiometric calibration and scan mirror correction procedures. The figure 9 indicates the main steps performed by the processing algorithms.

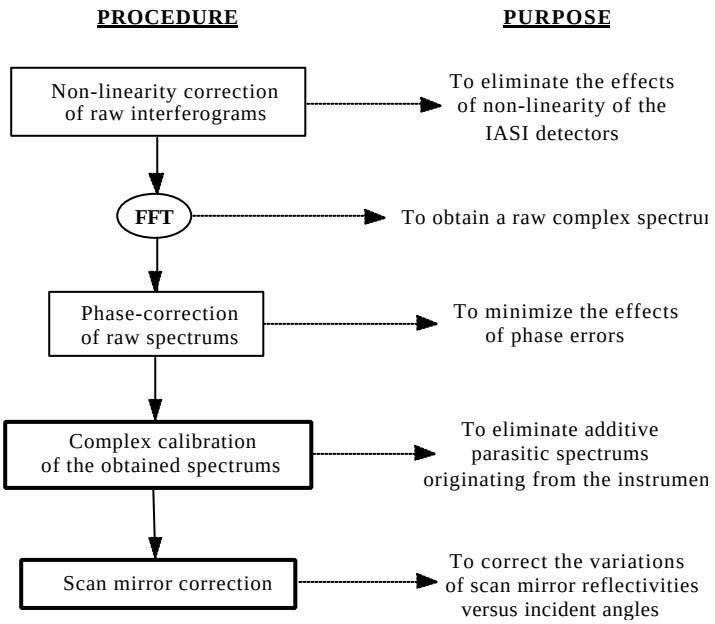

Figure 9 : Summary of the main correction algorithms implemented within the instrument

The study of the detector non-linearity and phase correction has already been described in [RD4]. The complex calibration procedure of the instrument is mainly based upon the work of Revercomb *et al*. [RD5]. It consists in subtracting from the measured spectrums (when observing the Earth's scene and the on-board reference blackbody), an offset spectrum obtained when the instrument is viewing at the cold space (assumed to be a blackbody with a temperature of 4 K). Thus additive parasitic emissions, that are supposed to originate mainly from the beamsplitter, are eliminated from the measured spectrums [RD2].

6.2 CURRENT RESULTS

The radiometric calibration performance may be affected by the radiometric noise, which is directly read from the outputs of the budget described in the paragraph 5. The other error items (calculated in terms of drift, bias, or noise, depending on their physical origin) included within the radiometric calibration budget are the following :

- Modelisation of the self-emission of the beamsplitter coating
- Modelisation of the self-emission of the other optical components
- Modelisation of the blackbody performances and of its environment
- Modelisation of the scan mirror reflectivity and of the residual error of its correction algorithm
- Preliminary modelisation of the straylight

The figure 10 summarises the radiometric calibration performance for a scene temperature of 280 K. The thick lines represent the specifications, while the narrow lines are the estimated performances of the instrument.

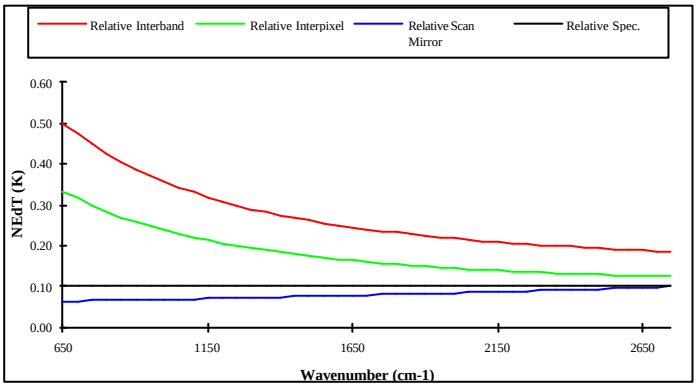

10.a)

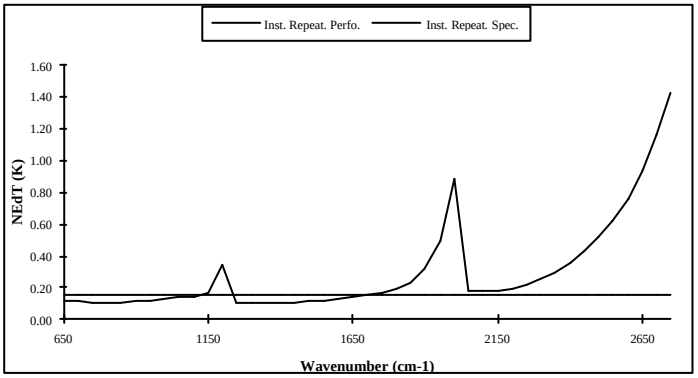

10.b)

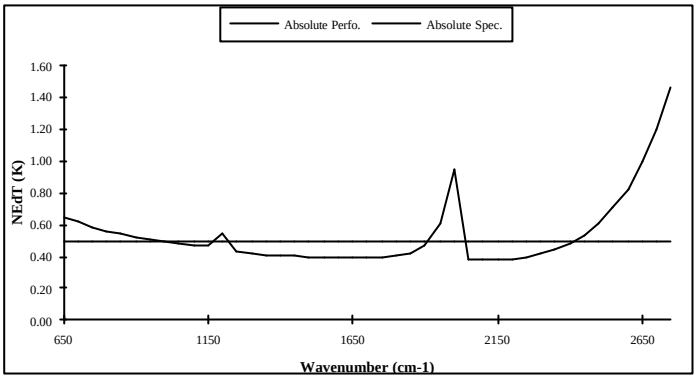

10.c)

Figure 10 : The instrument radiometric calibration budget
10.a) Relative interband, interpixel, and Scan mirror accuracies
10.b) Instantaneous repeatability 10.c) Absolute accuracy

The repeatability and absolute accuracy performances are globally achieved, excepting some limited domains located at the end of each spectral band. This is due to the radiometric noise influence. In addition the three most important errors terms are related to the hot reference blackbody (spatial and spectral non-homogeneities of the emissivity, and temperature estimate error).

7. CONCLUSION

In this paper were presented the performance requirements of the IASI instrument, and the basic principles on which they are evaluated. A modular architecture using several different models that are linked together was preferred to the global ray-tracing simulation approach. This was made possible because the IASI instrument performance (both spectral or radiometric) closely depend on the characteristic interferogram contrast function and instrument self-apodization function, that may be evaluated separately. Calculating these two functions only requires a minimum amount of ray-tracing computations, which are performed using a dedicated geometrical model.

The four main models developed so far (geometrical ray-tracing program, spectral performance model, radiometric noise and radiometric calibration budgets) now constitute a set of evoluted simulation tools that will be intensively used in order to define the specifications of critical subsystems or components (such as the interferometer and its beamsplitter).

8. REFERENCES

[RD1] P. Javelle, “IASI instrument overview”, Proceedings of the 5th Workshop on ASSFTS, November 30th - December 2nd, 1994, Tokyo

[RD2] K. Dohlen, F. Hénault, D. Scheidel, D. Siméoni, F. Cayla, G. Challon, P. Javelle, “Infrared Atmospheric Sounding Interferometer”, Proceedings of the 5th Workshop on ASSFTS, November 30th - December 2nd, 1994, Tokyo

[RD3] P. Griffiths, J. de Haseth, “Fourier-transform infrared spectrometry”, Wiley-Interscience, New York, 1986

[RD4] S. Muller, “Correction of non-linearity and phase error in IASI interferograms”, Proceedings of the 5th Workshop on ASSFTS, November 30th - December 2nd, 1994, Tokyo

[RD5] H. Revercomb, H. Buijs, H. Howell, D. LaPorte, W. Smith, L. Sromovski “Radiometric calibration of IR Fourier transform spectrometers : solution to a problem with the High-Resolution Interferometer Sounder”, Applied Optics, Vol. 27, n° 15, 1 August 1988